Article

Study on Stress–Strain Relationship of Coir Fiber-Reinforced Red Clay Based on Duncan–Chang Model

Xueliang Jiang [1,2], Jiahui Guo [2,*], Hui Yang [1,2], Shufeng Bao [1], Changping Wen [2] and Jiayu Chen [2]

[1] School of Civil and Engineering Management, Guangzhou Maritime University, Guangzhou 510725, China
[2] School of Civil Engineering, Central South University of Forestry and Technology, Changsha 410004, China
* Correspondence: jiahuiguo7@163.com; Tel.: +86-18774893172

Abstract: Compared with other natural fibers, coir fiber has good strength characteristics and long-term anti-biodegradation ability. At present, most studies on randomly distributed coir fiber-reinforced soil have focused on cohesionless soil or granular soil. In this paper, the influence of randomly distributed coir fiber on the deviatoric stress and shear strength index of red clay with different fiber content was assessed by a consolidated undrained (CU) triaxial compression test. Since the hyperbolic variational character of the stress–strain relation of the samples conformed to the hyperbolic hypothesis of the Duncan–Chang model of nonlinear elastic model, the Duncan–Chang model was used to fit it, and the influences of fiber content and confining pressure on the parameters of the Duncan–Chang model were studied. The fiber content was determined by testing to be 0%, 0.2%, 0.25%, 0.3%, 0.35% and 0.4% of the dry soil mass. It has been found that coir fiber distributed in a random radial manner can significantly increase the deviatoric stress of red clay, and thus can be effectively used in the case of soil and fiber mixing. The cohesion of the red clay first increases and then decreases with the increase in fiber content, with an optimum content of 0.3%. The internal friction angle changes little with increasing fiber content.

Keywords: triaxial test; coir fiber; stress–strain relationship; shear strength; Duncan–Chang model

1. Introduction

In the field of geotechnical engineering, in order to pursue harmony with nature and practice the concept of environmental protection, researchers have engaged in extensive exploration and achieved certain research results [1–20]. One of the exploration paths is to find natural materials and combine them with soil to form biomass fiber-reinforced soil. As a renewable and environmentally friendly material, coir fiber has a certain tensile strength and elongation, as well as water resistance, mildew resistance, insect resistance, and non-breakable and non-perishable properties. Compared with other natural fibers, coir fiber has a longer life [21] and can even be used as a suitable medium for plant growth due to its high lignin content (about 46%).Using coir fiber as a reinforcing material can not only improve the strength and deformation resistance of the reinforced soil but also reduce the project cost. Therefore, such soil is a good biomass fiber-reinforced material, and it can also be applied to slopes, roadbeds, and other engineering practices. M. Suhendra et al. [22] used coir fiber to reinforce slopes and found that it could generate additional shear strength. Sheela Y. et al. [23] conducted a long-term comparative analysis of reinforced and unreinforced roads in five areas and found that the use of coconut-shell geotextiles to reinforce roads can reduce road deflection. Rajeswari et al. [24] used coir fiber to reinforce sand and found that the ultimate bearing capacity and settlement characteristics of the foundation on fiber-reinforced sand were significantly improved. G. Narendra Goud et al. [25] used coconut shell pith and lime to improve the expansion characteristics of expansive soil, making it suitable for the construction of flexible pavement. The fiber-reinforced soil-live tree pile slope supporting structure studied by our research group is

aimed at ensuring the short-term stability of slopes by exerting the reinforcement effect formed between the coir fiber and the filled soil. The long-term stability of the slope is guaranteed by the root-anchoring and anti-sliding effect [26,27] after the root system of the living tree pile is developed. Therefore, it is very important to study the mechanical properties and constitutive model of coir fiber-reinforced soil for the short-term stability of a slope. In addition, chemical treatments such as alkali treatment, brine treatment, acetylation treatment, benzoylation of the fiber and permanganate treatment [28] can be used to make the fiber less susceptible to corrosion. Gu et al. [29] used NaOH and CCl_4 to treat coir fiber and found that NaOH and CCl_4 could effectively improve the cohesion and tensile properties of the fiber. Anggraini et al. [30] adopted a nano treatment method to improve the durability and shear strength of coir fiber.

To investigate the mechanical properties of coir fiber-reinforced soil, Qin et al. [31] studied the reinforcement effect and variation law of coir fiber soil under different reinforcement conditions by using an indoor triaxial test. G. L. Sivakumar Babu et al. [32] added coir fiber to expansive soils and investigated the laws of coir fiber content, surrounding pressure, and fiber diameter on strength using a triaxial shear test. S. M. Dasaka et al. [33] studied the influence of the length and quantity of coir fiber on soil shear strength and found that coir fiber can effectively solve many short-term stability problems related to shear strength and permeability in geotechnical engineering. Widianti A. et al. [34] added coir fiber to expansive soil and investigated the effect of waste coir fiber content on the stress–strain relationship, shear strength parameters, and elastic modulus of the mixture. Jishnu et al. [28] studied the mechanical properties of coconut leaf-reinforced soil with a triaxial shear test and found that coconut leaf is a good reinforcement material for enhancing engineering performance and can be successfully used in various civil engineering applications such as slopes. Kar et al. [35] used coir fiber as a reinforcement material and carried out direct shear tests, unconfined compressive strength tests, and consolidation tests to study the strength and compressibility of fiber-reinforced soil. Maliakal et al. [36] found that randomly distributed coir fiber can significantly improve the shear strength of clay through a series of consolidated undrained triaxial compression tests. A. Diambra et al. [37] established a new procedure to determine the directional distribution of fibers in reinforced sand samples and found that the directional distribution of fibers was far from isotropic. Stefania et al. [38] analyzed the influence of a small number of fibers with a high aspect ratio on sandy gravel through tests in a large triaxial instrument.

The constitutive model of soil was established to better reflect the strength and deformation relationship of soil. Since the Duncan–Chang model has fewer parameters and is easy to determine, it can better reflect the nonlinear characteristics of the soil, so it is widely used in mechanical properties analysis and numerical simulation of fiber-reinforced soil. Deng et al. [39] studied the influence of fiber content on the Duncan–Chang model parameters of polypropylene fiber cement silty clay by triaxial compression test. Feng et al. [40] constructed a modified Duncan–Chang model that can reflect the influence of the polyester fiber yarn blending ratio through the analysis of triaxial shear test data. Zhao et al. [41] studied the strength characteristics of fiber-reinforced soil under different polypropylene fiber content and confining pressure through triaxial tests, and used the Duncan–Chang model to describe its stress–strain relationship and proposed a calculation method to determine the model parameters. Hu et al. [42] studied the influence of polyvinyl alcohol fiber on the engineering properties of solidified silt and Duncan–Chang model parameters through a series of triaxial tests. Zhang et al. [43] mixed polypropylene fibers with different mass ratios into coal gangue-modified expansive soil for triaxial consolidation drainage tests and used MATLAB software to obtain the fitting function of fiber content and confining pressure to model parameters *a* and *b*, and verified the fitting degree of the Duncan–Chang model.

Most of the published literature on the reinforcement of soil with randomly distributed coir fiber is currently related to the reinforcement of non-cohesive or granular soil. There has been limited research on the use of randomly distributed coir fiber in cohesive soil, and

very little work has been done in combination with the Duncan–Chang model. In order to make coir fiber more applicable to slope engineering, this paper mainly discusses the stress–strain relationship and strength characteristics of coir fiber-reinforced soil under different fiber content and confining pressure through the consolidated undrained triaxial shear test and studies the influence of fiber content and confining pressure on Duncan–Chang model parameters.

2. Materials and Methods

2.1. Test Materials

In this paper, the test soil was taken from a school soil in Tianxin District, Changsha City, Hunan Province. After the soil samples were taken back to the laboratory, the basic physical properties were measured according to the "Highway Geotechnical Test Procedures" (JTG3430-2020). The results are shown in Table 1 and Figure 1. To ensure the homogeneity of the reinforced soil samples made, the soil collected on site was air-dried and crushed, and then passed through a 2 mm sieve. Coir fiber is a type of long fiber with a multi-cell aggregation structure. Its diameter is 100–450 μm, length is 10–25 cm, density is 1.12 g/cm^3.

Table 1. Basic physical parameters of red clay.

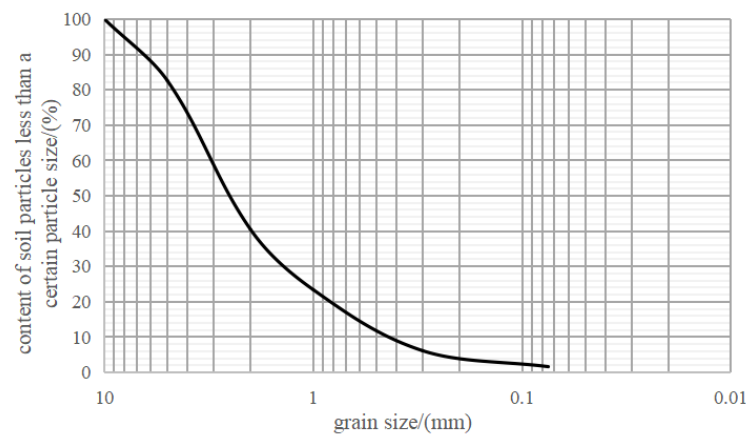| Specific Gravity	Maximum Dry Density /(g·cm^{-3})	Optimum Moisture Content /%	Liquid Limit ω_L/%	Plastic Limit ω_P/%	Plasticity Index I_P
2.74	1.70	20.0%	49.0	22.7	26.3

Figure 1. Particle gradation curve of red clay.

2.2. Test Methods

The influence of the coir fiber content on the strength and deformation of the red clay was studied using a soil static triaxial apparatus. Firstly, the range of coir fiber content was determined by consulting the relevant literature. Secondly, after a series of tests, it was found that the coir fiber content with an interval of 0.05% was more in line with the test requirements. Therefore, the coir fiber content was determined to be 0%, 0.2%, 0.25%, 0.3%, 0.35%, and 0.4% of the dry soil mass, as shown in Figure 2. The consolidated undrained (CU) test method was used in the test. The confining pressures of 100 kPa, 200 kPa, 300 kPa, and 400 kPa were applied to each group of samples with different fiber contents, and the shear rate was set to 0.08 mm/min. Three groups of parallel tests were carried out under each test condition. The peak point of the stress–strain relationship curve was taken as the failure standard. When there was no peak point, the axial strain reached 15%, which was regarded as the failure of the specimen.

Figure 2. Coir fiber incorporated in soil.

2.3. Sample Preparation

According to the requirements of the "Highway Geotechnical Test Procedure" (JTG3430-2020), the specimens for this test were prepared in six batches according to the different doses, mixed, maintained, and saturated under the same conditions. The soil was prepared under the condition that the optimal moisture content obtained from the compaction test was 20%. After preparation, the soil was put into a plastic bag and placed in a moisturizing dish for sealing and curing for 24 h so that the moisture would be evenly distributed. The triaxial sample for the test was 39.1 mm in diameter and 80 mm in height. The dispersed coir fiber was mixed into the soil sample according to the proposed fiber mix ratio and thoroughly and evenly mixed. Five layers were compacted, 27 under each layer, to ensure that all five layers of the sample contained a random radial distribution of coir fiber. Finally, a vacuum saturation device was used to saturate the sample. The prepared sample is shown in Figure 3 and the sample during loading is shown in Figure 4.
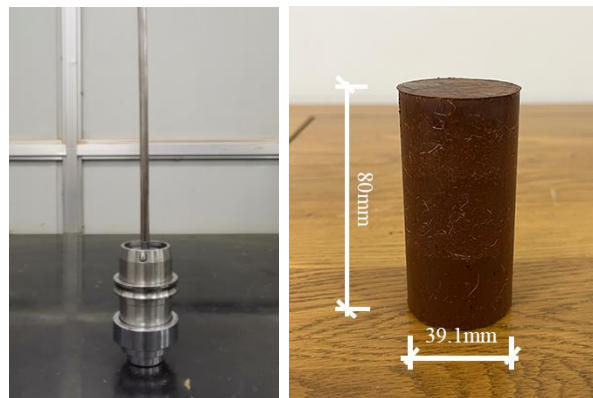

Figure 3. Sample preparation.

Figure 4. Sample under loading.

3. Experimental Results and Analyses

3.1. Stress–Strain Relationship

By sorting out the triaxial test results for plain soil and coir fiber-reinforced soil samples, the stress–strain curves of each sample could be obtained by taking the axial strain ε_1 as the abscissa and the principal stress difference $\sigma_1 - \sigma_3$ as the ordinate, and the stress–strain curves of each sample could be analyzed, as shown in Figure 5.
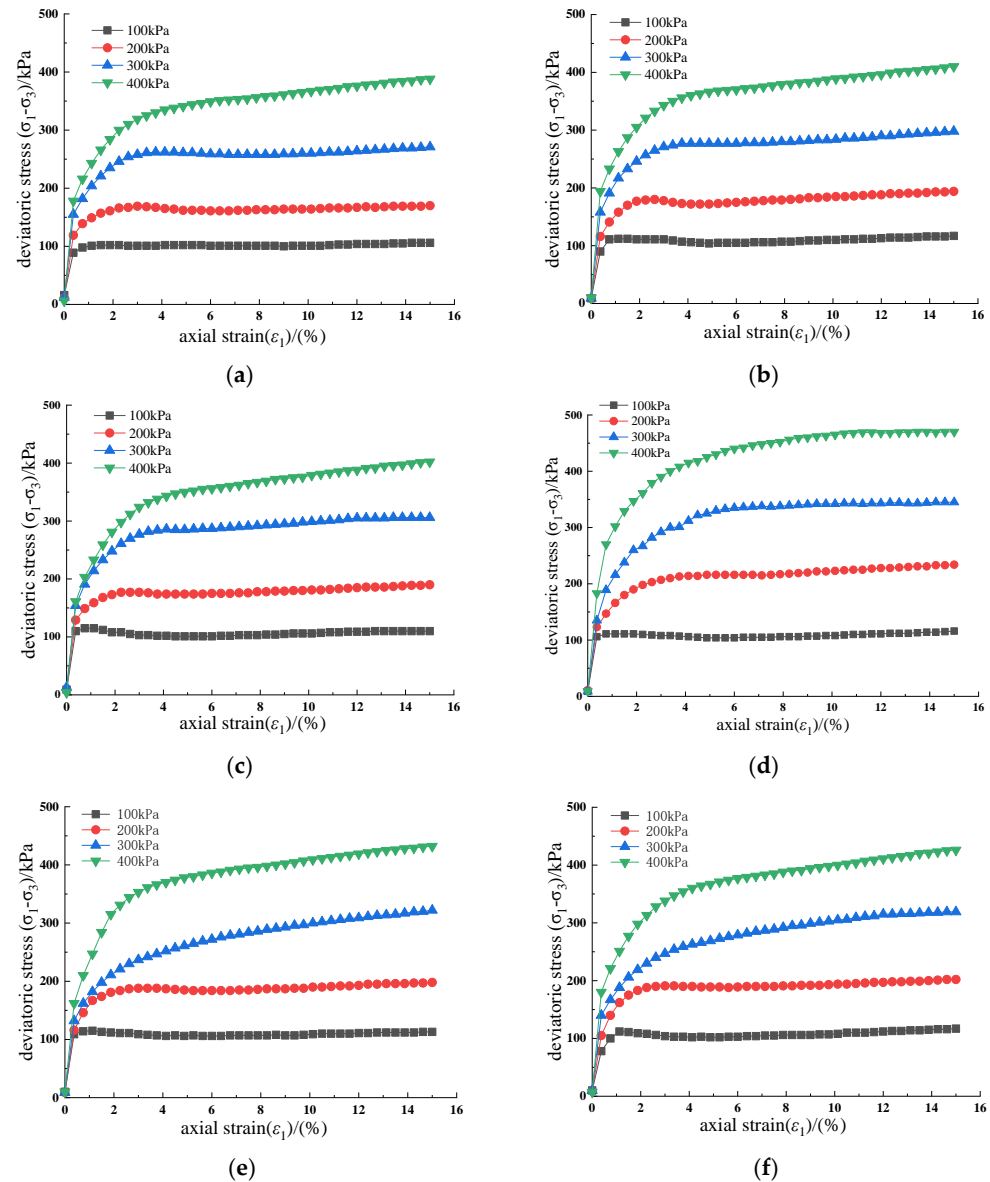

Figure 5. Relation curve between principal stress difference and axial strain. (**a**) 0% coir fiber; (**b**) 0.2% coir fiber; (**c**) 0.25% coir fiber; (**d**) 0.3% coir fiber; (**e**) 0.35% coir fiber; (**f**) 0.4% coir fiber.

As can be seen from Figure 5:

(1) Under different confining pressures and different fiber contents, the stress–strain relationship curves of plain soil and coir fiber-reinforced soil have similar trends, both of which are hyperbolic. With the increase in axial strain, the rate of increase in deviatoric stress decreases gradually, and the final deviatoric stress tends to a stable value. The stress–strain curve shows a typical strain-hardening type.

(2) Compared with plain soil, the peak deviatoric stress of five coir fiber-reinforced soil samples with different levels of fiber content increased substantially, indicating that the addition of coir fiber can affect the strength and deformation resistance of soil.

(3) Under low confining pressure (100 kPa, 200 kPa), the peak deviatoric stress of reinforced soil with different levels of coir fiber content shows little difference, indicating that the deviatoric stress is less affected by confining pressure under low confining pressure. Under high confining pressure (300 kPa, 400 kPa), the peak deviatoric stress of coir fiber-reinforced soil increases first and then decreases with the increase in fiber content, that is, there is an optimal coir fiber content. When the fiber content is 0.3%, the peak deviatoric stress reaches the maximum, and the reinforcement effect is the best. When the fiber content is too much, the fiber in the soil will be gathered together, such that the degree of occlusion and friction between the soil and the fiber becomes low, and it is easy to form penetrating cracks in the sample, which destroys the integrity of the soil due to the existence of potential failure surfaces.

(4) When the axial strain of the soil is small ($\varepsilon_1 < 1\%$), the stress and strain curves of the plain soil and the coir fiber-reinforced soil are basically equivalent, indicating that the coir fiber cannot play a good role under a small strain. This is mainly because when the soil deformation is small, the external force is also small, the occlusal friction between the soil and the fiber is weak, the cohesion of the soil itself is not much enhanced, and the degree of fiber bending in the soil is not enough, and the spatial constraint effect on the soil is weak, so the reinforcement effect is not obvious. With the increase in axial strain ε_1, the deviatoric stress of coir fiber-reinforced soil increases rapidly, and the greater the confining pressure, the greater the increase in the deviatoric stress, indicating that in the case of a certain small strain, coir fiber can play an early role in inhibiting the deformation of the soil, and the reinforcement effect of fiber soil is obviously reflected. When the axial strain reaches a certain value ($\varepsilon_1 > 4\%$), under the same fiber content, the greater the confining pressure, the greater the corresponding deviatoric stress. This is because there are more voids in the soil. The larger the confining pressure, the faster the void closure, the stronger the lateral restraint force, and the greater the deviatoric stress. From Figure 6, it can be seen that the pore pressure of the coir fiber-reinforced red clay sample increases to varying degrees compared with the plain soil. According to the effective stress principle of Terzaghi, $\sigma = \sigma' + u$, it can be known through calculation that although the pore water pressure u is increasing, the total stress is increasing faster, thus the effective stress σ' is still increasing from the overall point of view, and, therefore, the deformation of the specimen is constrained.
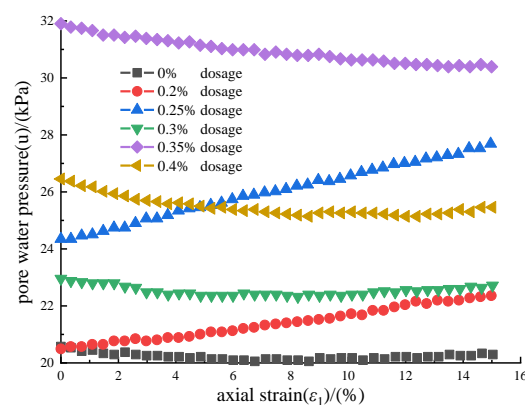

Figure 6. Relation curve between pore water pressure and axial strain at 300 kPa.

(5) Under the same fiber content, the deviatoric stress of soil increases obviously with the increase in confining pressure. Taking fiber content of 0.3% as an example, the deviatoric stress of soil under confining pressure of 100 kPa, 200 kPa, 300 kPa, and

400 kPa is 115 kPa, 234 kPa, 345 kPa, and 457 kPa, respectively. The deviatoric stress of 400 kPa is 297.39% higher than that of 100 kPa, which indicates that increasing confining pressure can improve the failure strength of the soil.

3.2. Shear Strength Parameters

The Mohr–Coulomb strength theory was used for the analysis based on the results of triaxial tests on the soil, and the Mohr stress circle at the time of sample damage and the shear strength envelope of the sample could be plotted as shown in Figure 7. According to the Mohr–Coulomb strength envelope of each specimen, the cohesive force c and the internal friction angle φ of each specimen were obtained by fitting as shown in Table 2.
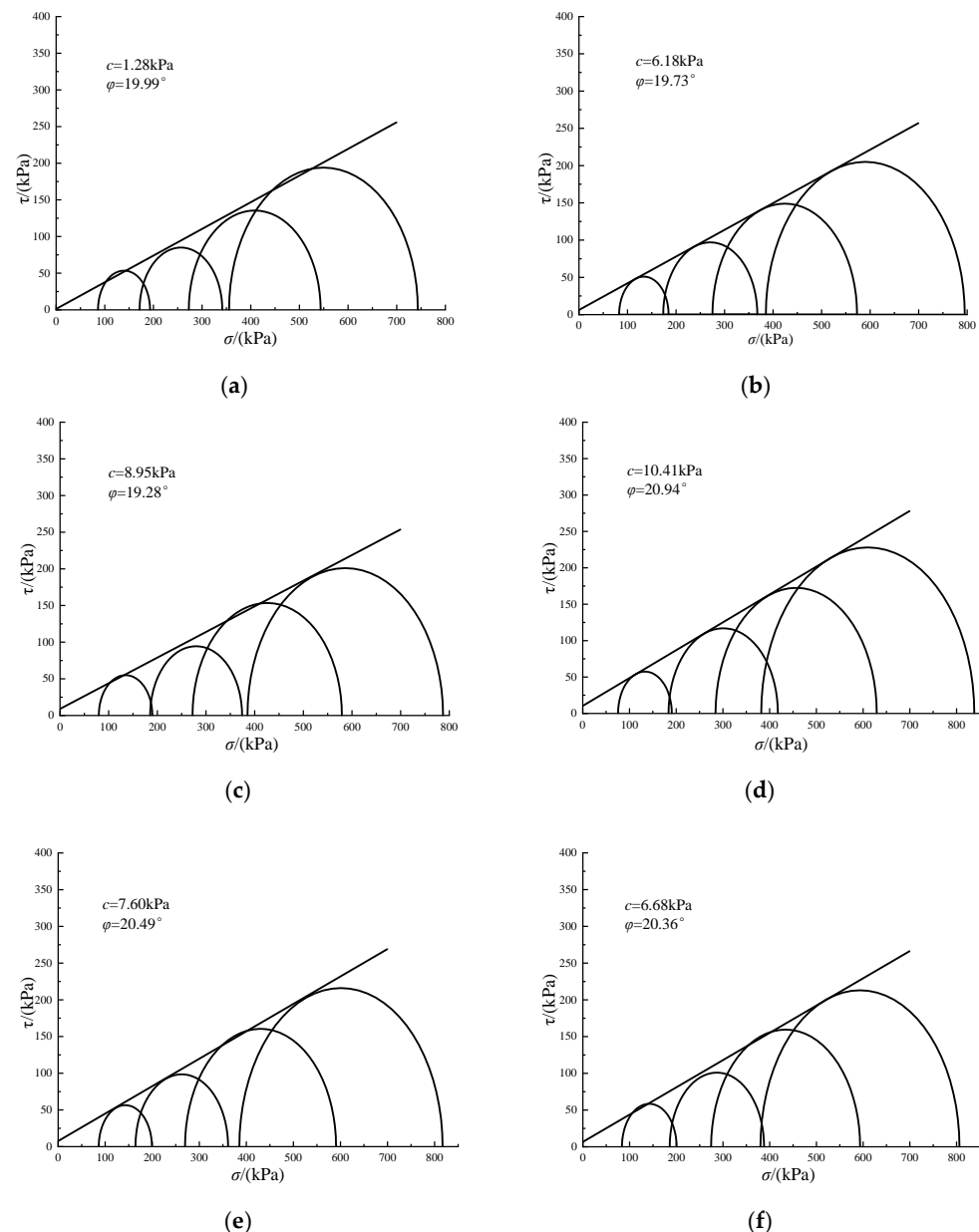

Figure 7. Mohr–Coulomb strength envelope of soil samples. (**a**) 0% coir fiber; (**b**) 0.2% coir fiber; (**c**) 0.25% coir fiber; (**d**) 0.3% coir fiber; (**e**) 0.35% coir fiber; (**f**) 0.4% coir fiber.

Table 2. Shear strength index of samples.

Fiber Content/%	c/kPa	φ/(°)
0	1.28	19.99
0.2	6.18	19.73
0.25	8.95	19.28
0.3	10.41	20.94
0.35	7.60	20.49
0.4	6.68	20.36

Figure 8 shows the influence of different levels of coir fiber content on the shear strength index of soil. For the consolidated undrained test of normally consolidated saturated soil, the cohesion is 0 in theory. Because the maximum dry density method was used in this test, partial cohesion also existed in the plain soil sample. From the diagram, it can be seen that with the increase in fiber content, the cohesion of coir fiber-reinforced soil showed a trend of increasing first and then decreasing. When the fiber content was 0.3%, the cohesion of the soil increased most significantly. Therefore, 0.3% fiber content was the optimal coir fiber content. With the increase in fiber content, the change in internal friction angle was not large, indicating that the friction characteristics of the fracture surface were basically unchanged after adding coir fiber to clay.
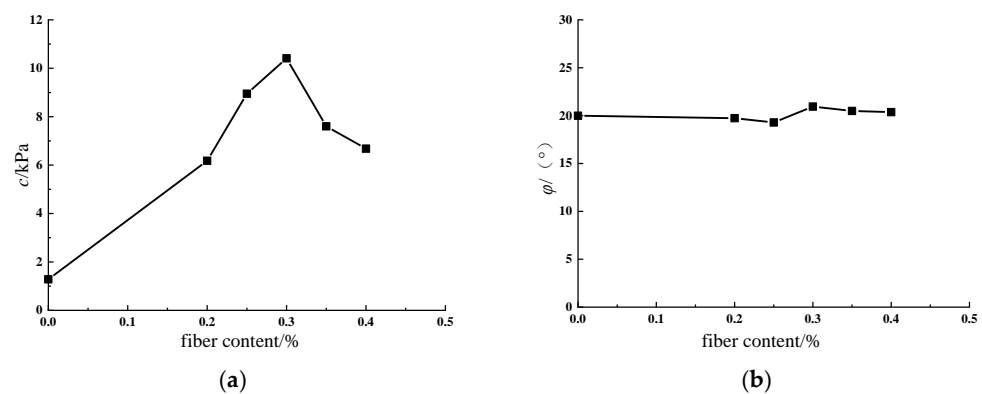

Figure 8. Variation in shear strength index with fiber content. (**a**) influence of fiber content on cohesion; (**b**) influence of fiber content on internal friction angle.

3.3. Failure Characteristics of Coir Fiber-Reinforced Soil

The failure mode of the coir fiber-reinforced soil sample is shown in Figure 9. From the diagram, it can be seen that the failure mode of the sample was a mainly bulging failure, that is, after the failure, the sample underwent lateral bulging, with large intermediate deformation, small ends, drum-shaped, and no obvious fracture surface. The deformation was gradual from the middle to the ends, and the shape was uniform. During the test, due to the friction between the two ends of the specimen and the upper and lower loading device, the restraint effect of the specimen from the two ends to the middle was gradually reduced, so the deformation characteristic of the middle was large, and that of the two was small. It can be found from the diagram that under the same fiber content, the larger the confining pressure, the greater the lateral binding force on the sample and the smaller the lateral bulging deformation. Under the same confining pressure, when the fiber content was 0%, the deformation of the sample was larger. The addition of the coir fiber could effectively reduce the lateral deformation of the sample, but the overall difference was not significant.
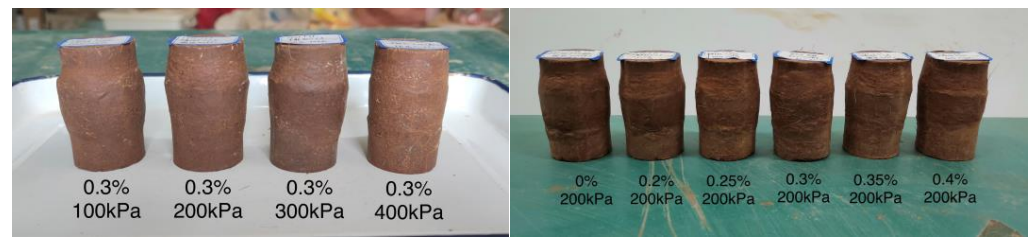
Figure 9. The failure mode of specimen under triaxial test.

4. Duncan–Chang Model and Parameter Analysis of Coir Fiber-Reinforced Red Clay

From Figure 5, it can be seen that the stress–strain relationship curve of coir fiber-reinforced red clay is a typical strain hardening type, which conforms to the hyperbolic hypothesis of the Duncan–Chang model of a nonlinear elastic model. The Duncan–Chang model is widely used in numerical simulation and engineering practice and has great research value. Therefore, this paper used this model to fit the stress–strain relationship of coir fiber-reinforced red clay, and obtained the influence of fiber content and confining pressure on the parameters of the Duncan–Chang model.

4.1. Establishment of the Model

In 1963, Kondner [44] proposed that the hyperbolic curve can be used to fit the curve according to the stress–strain relationship curve of a large number of soil triaxial tests. The hyperbolic equation is shown in Equation (1). Duncan et al. proposed a widely used incremental elastic model based on this hyperbolic stress–strain relationship, which is called Duncan–Chang model.

$$\sigma_1 - \sigma_3 = \frac{\varepsilon_a}{a + b\varepsilon_a} \tag{1}$$

In the formula: σ_1 and σ_3 are large and small principal stresses, respectively; a and b are parameters related to soil properties; σ_a is axial strain. For the conventional triaxial test, $\sigma_a = \sigma_1$.

By transforming Equation (1), we can obtain:

$$\frac{\varepsilon_1}{\sigma_1 - \sigma_3} = a + b\varepsilon_1 \tag{2}$$

In conventional triaxial tests, since $d\sigma_1 = d\sigma_2 = 0$, the tangent modulus is

$$E_t = \frac{d(\sigma_1 - \sigma_3)}{d\varepsilon_1} = \frac{a}{(a + b\varepsilon_1)^2} \tag{3}$$

According to Equation (3), when $\varepsilon_1 = 0$ ε_1, the initial tangent modulus E_i $E_t = E_i$ can be obtained. Then, the initial deformation modulus E_i is

$$E_i = E_t\bigg|_{\varepsilon_1=0} = \frac{a}{(a + b\varepsilon_1)^2}\bigg|_{\varepsilon_1=0} = \frac{1}{a} \tag{4}$$

The formula shows that the parameter a represents the reciprocal of the initial deformation modulus E_i.

According to Equation (2), when $\varepsilon_1 \to \infty$, the limit deviatoric stress difference $(\sigma_1 - \sigma_3)_{ult}$ is

$$(\sigma_1 - \sigma_3)_{ult} = \lim_{\varepsilon_1 \to \infty}(\sigma_1 - \sigma_3) = \lim_{\varepsilon_1 \to \infty}\frac{\varepsilon_1}{a + b\varepsilon_1} = \frac{1}{b} \tag{5}$$

This formula shows that the parameter b represents the reciprocal of the limit deviatoric stress $(\sigma_1 - \sigma_3)_{ult}$ corresponding to the asymptote of the $(\sigma_1 - \sigma_3) \sim \varepsilon_1$ hyperbola.

In the hyperbolic stress–strain relationship, the strength $(\sigma_1-\sigma_3)_f$ of the specimen at failure usually does not reach the ultimate deviatoric stress $(\sigma_1-\sigma_3)_{ult}$, so the failure ratio R_f can be defined as

$$R_f = \frac{(\sigma_1-\sigma_3)_f}{(\sigma_1-\sigma_3)_{ult}} \tag{6}$$

Substituting Equations (4)–(6) into Equation (3), the expression of tangent deformation modulus E_t is

$$E_t = E_i \left[1 - R_f \frac{\sigma_1 - \sigma_3}{(\sigma_1 - \sigma_3)_f} \right]^2 \tag{7}$$

4.2. Parameter Analysis

The above triaxial shear test data are organized by *a–b*, and the results obtained are shown in Figure 10. According to the test analysis, the $\frac{\varepsilon_1}{\sigma_1-\sigma_3} \sim \varepsilon_1$ of coir fiber-reinforced cohesive soil is approximately a first-order linear relationship, indicating that the $(\sigma_1-\sigma_3) \sim \varepsilon_1$ hyperbolic relationship can be well established. The strength and tangent elastic modulus of coir fiber-reinforced cohesive soil can be reasonably determined according to the Duncan–Chang model, which conforms to the strain-hardening relationship. Parameters *a* and *b* are the intercept and slope of the curve $\frac{\varepsilon_1}{\sigma_1-\sigma_3} \sim \varepsilon_1$, respectively.
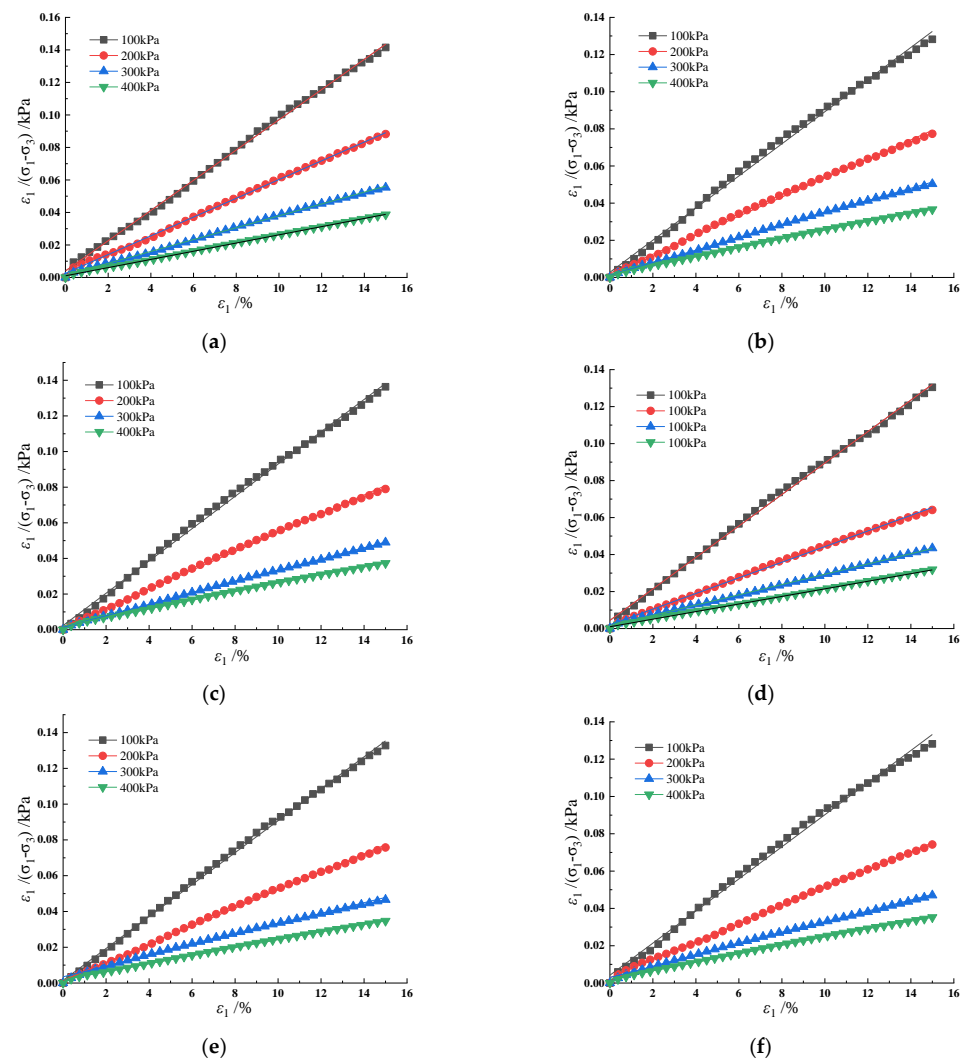

Figure 10. $\varepsilon_1 / (\sigma_1-\sigma_3) \sim \varepsilon_1$ curve of sample. (**a**) 0% coir fiber; (**b**) 0.2% coir fiber; (**c**) 0.25% coir fiber; (**d**) 0.3% coir fiber; (**e**) 0.35% coir fiber; (**f**) 0.4% coir fiber.

By fitting and calculating the data of unreinforced fiber soil and coir fiber-reinforced soil, this paper gives the Duncan–Chang model parameters of the specimens with different fiber content under different confining pressures, as shown in Table 3. It can be seen from the table that under the same fiber content, the parameters *a* and *b* gradually decrease with the increase in confining pressure. Contrarily, the initial deformation modulus E_i and the ultimate deviatoric stress $(\sigma_1-\sigma_3)_{ult}$ of the sample increase with the increase in confining pressure, while the failure ratio R_f is in a fluctuating state.

Table 3. Tangent deformation modulus and related parameters.

Fiber Content (%)	Confining Pressure (kPa)	Parameter *a*	Parameter *b*	E_i ($\times 10^3$ kPa)	$(\sigma_1-\sigma_3)_{ult}$ (kPa)	R_f
0	100	0.00471	0.00930	212.31	107.53	0.9951
	200	0.00386	0.00577	259.07	173.31	0.9809
	300	0.00315	0.00365	317.46	273.97	0.9892
	400	0.00223	0.00252	448.43	396.83	0.9777
0.2	100	0.00418	0.00850	239.23	117.61	0.8673
	200	0.00207	0.00513	483.09	194.93	0.9952
	300	0.00160	0.00333	625.00	300.30	0.9923
	400	0.00127	0.00238	787.40	420.17	0.9758
0.25	100	0.00385	0.00906	259.74	110.38	0.9966
	200	0.00177	0.00527	564.97	189.75	0.9960
	300	0.00149	0.00318	671.14	314.47	0.9762
	400	0.00113	0.00240	884.96	416.67	0.9648
0.3	100	0.00330	0.00851	303.03	117.51	0.9786
	200	0.00202	0.00422	495.05	236.97	0.9875
	300	0.00139	0.00278	719.42	359.71	0.9591
	400	0.00087	0.00205	1149.43	487.80	0.9635
0.35	100	0.00453	0.00862	220.75	115.98	0.9743
	200	0.00279	0.00505	358.43	198.02	0.9948
	300	0.00187	0.00296	534.76	337.84	0.9502
	400	0.00138	0.00223	724.64	448.43	0.9634
0.4	100	0.00460	0.00826	217.39	121.05	0.9665
	200	0.00355	0.00482	281.69	207.47	0.9736
	300	0.00298	0.00297	335.57	336.70	0.9474
	400	0.00201	0.00227	497.51	440.53	0.9670

In 1963, Janbu proposed an empirical formula reflecting the relationship between initial tangent modulus E_i and confining pressure:

$$E_i = K p_a \left(\frac{\sigma_3}{p_a} \right)^n \tag{8}$$

In the formula, K and n are test constants, and P_a is atmospheric pressure, generally taken as 101.33 kPa.

It can be seen from Equation (8) that $\log_{10} \frac{E_i}{p_a} = \log_{10} K + n \log_{10} \frac{\sigma_3}{p_a}$, that is, $\log_{10} \frac{E_i}{p_a} \sim \log_{10} \frac{\sigma_3}{p_a}$ is a linear relationship. The $\log_{10} \frac{E_i}{p_a} \sim \log_{10} \frac{\sigma_3}{p_a}$ relationship curves of samples with different levels of fiber content were drawn in the coordinate system, and linear fitting was carried out. The fitting results are shown in Figure 11. From the diagram, it can be found that on the one hand, the initial tangent modulus increases with the increase in confining pressure; on the other hand, the initial tangent modulus increases first and then decreases with the increase in fiber content, but both are higher than the initial tangent modulus of unreinforced fiber soil. This shows that adding coir fiber to the soil can improve the initial tangent modulus of the soil, and when the fiber content is 0.3%, the initial tangent modulus reaches its highest value.
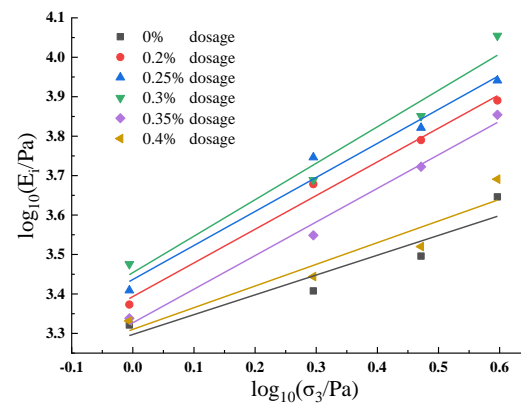
Figure 11. Relationship curve between initial tangent modulus and confining pressure of sample.

5. Discussion

A. Widianti et al. [34] added coir fiber to expansive soil and found that under the same confining pressure, the sample had maximum deviatoric stress when the fiber content was 0.6%, which was similar to our research results. The reason for the difference in the optimal fiber content between the two studies may be due to the different types of reinforced soil tested. In addition, our study of coir fiber-reinforced red clay showed that its deviatoric stress was higher than that of the coir fiber-reinforced expansive soil studied by A. Widianti et al. [34]. The reason may be due to the different test methods. Our study adopted the consolidated undrained test method, and the strength of the consolidated soil was higher than that of the unconsolidated soil. A. Widianti et al. [34] found that the cohesion of the soil was highest when the fiber content was 0.6%. When it exceeded 0.6%, the cohesion of the soil would decrease. This trend is the same as the change rule in our study, which found that the cohesion of soil increased first and then decreased with increasing fiber content, and reached a maximum at 0.3%.

All of the formulas of the Duncan–Chang model are calculated under the condition that σ_3 is constant, that is to say, it is obtained under the condition that the lateral stress is constant and the axial stress is increased. The problems of stress path and dilatancy are not considered, and the influence of the intermediate principal stress cannot be reflected, which is its limitation. In this paper, samples with a diameter of 39.1 mm and a height of 80 mm were used for research. If conditions permit in the future, samples with larger sizes can be used for research, such as 69.1 mm × *125 mm, which can better reflect the stress and deformation of coir fiber-reinforced red clay in practical engineering. The deformation mechanism of coir fiber in soil can also be further investigated by microscopic experiments.

6. Conclusions

In this paper, the influence of coir fiber content on the strength characteristics of red clay was studied by the consolidated undrained triaxial test, and the parameters were analyzed in combination with the Duncan–Chang model. This provides an important reference value for the strength theory of coir fiber-reinforced red clay. The following conclusions were drawn:

(1) The strength characteristics of red clay can be effectively improved by adding coir fiber to the soil. Under the optimal fiber content, the failure strength of the sample is nearly three times that of plain soil.

(2) When the axial strain is small, the stress–strain relationship curves of the plain soil and the coir fiber-reinforced red clay are consistent, indicating that the reinforcement effect is not obvious at this time. With the increase in axial strain, the occlusal friction between the soil and the fiber and the tensile resistance of the fiber gradually play a role, which improves the shear strength of the soil and increases the deviatoric stress of different samples.

(3) Compared with plain soil, the cohesion of red clay mixed with fiber increases by 4.9~9.13 kPa, and reaches the maximum when the fiber content is 0.3%, while the internal friction angle of red clay mixed with fiber is not much different from that of plain soil.

(4) Under the same fiber content, the parameters *a* and *b* gradually decrease with the increase in confining pressure, and the initial deformation modulus E_i and ultimate deviator stress $(\sigma_1 - \sigma_3)_{ult}$ of the sample increase with the increase in confining pressure. Additionally, the initial tangent modulus E_i increases first and then decreases with the continuous increase in fiber content. The rule of change is in line with the test situation and has guiding significance.

Author Contributions: Conceptualization, X.J.; Methodology, C.W.; Validation, H.Y.; Formal analysis, J.C.; Investigation, S.B.; Writing—original draft, J.G. All authors have read and agreed to the published version of the manuscript.

Institutional Review Board Statement: Not applicable.

Informed Consent Statement: Not applicable.

Data Availability Statement: The original contributions presented in the study are included in the article. Further inquiries can be directed to the corresponding author.

Conflicts of Interest: The authors declare no conflict of interest.

References

1. Li, C.; Papel, T. Analyzing the role of environmental technologies and environmental policy stringency on green growth in China. *Environ. Sci. Pollut. Res.* **2022**, *29*, 55630–55638. [CrossRef]
2. Liu, X.; Nie, W. Study on the coupling coordination mechanism of green technology innovation, environmental regulation, and green finance. *Environ. Sci. Pollut. Res.* **2022**, *29*, 71796–71809. [CrossRef] [PubMed]
3. Yuan, Z.G.; Zhao, J.T.; Li, S.Q.; Jiang, Z.; Huang, F. A Unified Solution for Surrounding Rock of Roadway Considering Seepage, Dilatancy, Strain-Softening and Intermediate Principal Stress. *Sustainability* **2022**, *14*, 8099. [CrossRef]
4. Fan, H.D.; Lu, Y.F.; Hu, Y.L.; Fang, J.; Lv, C.; Xu, C.; Feng, X.; Liu, Y. A Landslide Susceptibility Evaluation of Highway Disasters Based on the Frequency Ratio Coupling Model. *Sustainability* **2022**, *14*, 7740. [CrossRef]
5. Zheng, C.S.; Jiang, B.Y.; Xue, S.; Chen, Z.; Li, H. Coalbed methane emissions and drainage methods in underground mining for mining safety and environmental benefits: A review. *Process Saf. Environ. Prot.* **2019**, *127*, 103–124. [CrossRef]
6. Liu, Y.; He, B.C.; Xie, J.; Lu, Y.; Zhang, L. Compatibility of geosynthetic clay liners at different temperatures. *J. Environ. Prot. Ecol.* **2021**, *22*, 2295–2306.
7. Zhu, C.G.; Long, S.C.; Zhang, J.X.; Wu, W.; Zhang, L. Time Series Multi-Sensors of Interferometry Synthetic Aperture Radar for Monitoring Ground Deformation. *Front. Environ. Sci.* **2022**, *10*, 929958. [CrossRef]
8. Huang, Z.A.; Huang, Y.; Yang, Z.J.; Zhang, J.; Zhang, Y.; Gao, Y.; Shao, Z. Study on the physicochemical characteristics and dust suppression performance of new type chemical dust suppressant for copper mine pavement. *Environ. Sci. Pollut. Res.* **2021**, *28*, 59640–59651. [CrossRef]
9. Zhang, Y.; Ren, B.Z.; Hursthouse, A.S.; Deng, R.; Hou, B. An Improved SWAT for Predicting Manganese Pollution Load at the Soil-Water Interface in a Manganese Mine Area. *Pol. J. Environ. Stud.* **2018**, *27*, 2357–2365. [CrossRef]
10. Zhao, Y.L.; Tang, J.Z.; Chen, Y.; Zhang, L.; Wang, W.; Wan, W.; Liao, J. Hydromechanical coupling tests for mechanical and permeability characteristics of fractured limestone in complete stress-strain process. *Environ. Earth Sci.* **2017**, *76*, 24. [CrossRef]
11. Yu, W.J.; Li, K.; Liu, Z.; An, B.; Wang, P.; Wu, H. Mechanical characteristics and deformation control of surrounding rock in weakly cemented siltstone. *Environ. Earth Sci.* **2021**, *80*, 337. [CrossRef]
12. Zhao, Y.L.; Luo, S.L.; Wang, Y.X.; Zhang, L.; Wan, W. Numerical Analysis of Karst Water Inrush and a Criterion for Establishing the Width of Water-resistant Rock Pillars. *Mine Water Environ.* **2017**, *36*, 508–519. [CrossRef]

13. Chen, C.H.; Peng, Z.S.; Gu, J.Y.; Peng, Y.; Huang, X.; Wu, L. Exploring Environmentally Friendly Biopolymer Material Effect on Soil Tensile and Compressive Behavior. *Int. J. Environ. Res. Public Health* **2020**, *17*, 9032. [CrossRef] [PubMed]
14. Luo, X.; Ren, B.Z.; Hursthouse, A.S.; Thacker, J.R.M.; Wang, Z. Soil from an Abandoned Manganese Mining Area (Hunan, China): Significance of Health Risk from Potentially Toxic Element Pollution and Its Spatial Context. *Int. J. Environ. Res. Public Health* **2020**, *17*, 6554. [CrossRef] [PubMed]
15. Liu, S.K.; Nie, Y.X.; Hu, W.; Ashiru, M.; Li, Z.; Zuo, J. The Influence of Mixing Degree between Coarse and Fine Particles on the Strength of Offshore and Coast Foundations. *Sustainability* **2022**, *14*, 9177. [CrossRef]
16. Wang, P.; Zhang, J.; Chen, Z.; Yang, X. Improvement of different biopolymers on electroosmotic consolidation of soil. *International J. Environ. Sci. Technol.* **2022**. [CrossRef]
17. Pacheco-Torgal, F.; Ivanov, V.; Karak, N.; Jonkers, H. *Biopolymers and Biotech Admixtures for Eco-Efficient Construction Materials*; Woodhead Publishing: Cambridge, UK, 2016.
18. Chang, I.; Prasidhi, A.K.; Im, J.; Shin, H.-D.; Cho, G.-C. Soil treatment using microbial biopolymers for anti-desertification purposes. *Geoderma* **2015**, *253*, 39–47. [CrossRef]
19. Prabakar, J.; Sridhar, R.S. Effect of random inclusion of sisal fibre on strength behaviour of soil. *Constr. Build. Mater.* **2002**, *16*, 123–131. [CrossRef]
20. Liu, J.L.; Hou, T.S.; Luo, Y.S.; Cui, Y.-X. Experimental Study on Unconsolidated Undrained Shear Strength Characteristics of Synthetic Cotton Fiber Reinforced Soil. *Geotech. Geol. Eng.* **2020**, *38*, 1773–1783. [CrossRef]
21. Sridhar, R. A Review on performance of coir fiber reinforced sand. *Int. J. Eng. Technol.* **2017**, *9*, 249–256. [CrossRef]
22. Suhendra, M.; Yunita, H.; Saleh, S.M. Coconut fiber strength test as a potential to prevent landslides on badlands. *IOP Conf. Ser. Mater. Sci. Eng.* **2020**, *933*, 012038. [CrossRef]
23. Evangeline, S.Y.; Sayida, M.K.; Girish, M.S. Long-Term Performance of Rural Roads Reinforced with Coir Geotextile—A Field Study. *J. Nat. Fibers* **2019**, *18*, 1419–1436. [CrossRef]
24. Rajeswari, J.S.; Sarkar, R.; Roy, N.; Bharti, S. D Bearing capacity of circular footing supported on coir fiber-reinforced soil. *Int. J. Geotech. Eng.* **2019**, *13*, 218–226. [CrossRef]
25. Goud, G.N.; Hyma, A.; Chandra, V.S.; Rani, R.S. Expansive soil stabilization with coir waste and lime for flexible pavement subgrade. *IOP Conf. Ser. Mater. Sci. Eng.* **2018**, *330*, 012130. [CrossRef]
26. Jiang, X.L.; Qian, Y.H.; Yang, H.; Xiao, Z.; Fan, W.; Zhu, Y.; Liu, W.; Guo, J. Model Test Studies on Slope Supported by Bamboo Anchor and Timber Frame Beam. *Geotech. Geol. Eng.* **2022**, *40*, 4327–4344. [CrossRef]
27. Zhu, Y.; Yang, H.; Liu, Y.; Jiang, X.; Deng, R.; Huang, L.; Yin, P.; Lai, G. Numerical Simulation of the Combined Slope Protection Effect of Living Stump and Bamboo Anchor. *Geotech. Geol. Eng.* **2022**, *40*, 635–645. [CrossRef]
28. Jishnu, V.P.; Sankar, N.; Chandrakaran, S. Strength behaviour of cohesionless soil reinforced with coconut leaf let as a natural material. *Mater. Today Proc.* **2020**, *31*, S340–S347. [CrossRef]
29. Huang, G. Tensile behaviours of the coir fiber and related composites after NaOH treatment. *Mater. Des.* **2009**, *30*, 3931–3934. [CrossRef]
30. Anggraini, V.; Asadi, A.; Farzadnia, N.; Jahangirian, H.; Huat, B.B.K. Reinforcement Benefits of Nanomodified Coir Fiber in Lime-Treated Marine Clay. *J. Mater. Civ. Eng.* **2016**, *28*, 06016005. [CrossRef]
31. Qin, W.S.; Li, G.F.; Hu, W.; Li, B.J.; Zou, G.H. Triaxial test study of coir fiber soil. *Sci. Technol. Eng.* **2017**, *17*, 272–276.
32. Sivakumar Babu, G.L.; Vasudevan, A.K.; Sayida, M.K. Use of Coir Fibers for Improving the Engineering Properties of Expansive Soils. *J. Nat. Fibers* **2008**, *5*, 61–75. [CrossRef]
33. Dasaka, S.M.; Sumesh, K.S. Effect of Coir Fiber on the Stress–Strain Behavior of a Reconstituted Fine-Grained Soil. *J. Nat. Fibers* **2011**, *8*, 189–204. [CrossRef]
34. Widianti, A.; Diana, W.; Alghifari, M.R. Shear Strength and Elastic Modulus Behavior of Coconut Fiber-Reinforced Expansive Soil. *IOP Conf. Ser. Mater. Sci. Eng.* **2021**, *1144*, 012043. [CrossRef]
35. Kar, R.; Pradhan, P. Strength and compressibility characteristics of randomly distributed fiber-reinforced soil. *Int. J. Geotech. Eng.* **2011**, *5*, 235–243. [CrossRef]
36. Maliakal, T.; Thiyyakkandi, S. Influence of Randomly Distributed Coir Fibers on Shear Strength of Clay. *Geotech. Geol. Eng.* **2013**, *31*, 425–433. [CrossRef]
37. Diambra, A.; Russell, A.R.; Ibraim, E.; Muir Wood, D. Determination of fibre orientation distribution in reinforced sands. *Géotechnique* **2007**, *57*, 623–628. [CrossRef]
38. Lirer, S.; Flora, A.; Consoli, N.C. Experimental Evidences of the Effect of Fibres in Reinforcing a Sandy Gravel. *Geotech. Geol. Eng.* **2012**, *30*, 75–83. [CrossRef]
39. Deng, L.F.; Ruan, B. Triaxial compression test of polypropylene fiber cement silty clay. *J. Railw. Sci. Eng.* **2019**, *16*, 1201–1206. [CrossRef]
40. Chu, F.; Luo, J.B.; Yang, W.P.; Shao, S.; Yu, Y.; Xu, C. Strength and Deformation Characteristics of Fiber Reinforced Longdong Loess and Experimental Study of Modified Duncan-Chang Model. In Proceedings of the 7th International Conference on Environmental Science and Civil Engineering (ESCE 2021), Nanchang, China, 9 January 2021; pp. 1104–1121. [CrossRef]
41. Zhao, Y.Y.; Ling, X.Z.; Gong, W.G.; Li, P.; Li, G.; Wang, L. Mechanical Properties of Fiber-Reinforced Soil under Triaxial Compression and Parameter Determination Based on the Duncan-Chang Model. *Appl. Sci.* **2020**, *10*, 9043. [CrossRef]

42. Hu, Y.Y.; Yu, Q.Z.; Zhang, C.J.; Qian, J.L.; Xie, J.Q. Duncan-Chang model of fiber reinforced silt solidified soil. *J. Zhejiang Univ. Eng.* **2017**, *51*, 1500–1508.

43. Zhang, Y.; He, G.H.; Yu, P.L. Strength Characteristics and Duncan-Chang Model Parameters of Expansive Soil Improved by Fiber Coal Gangue. *Sci. Technol. Eng.* **2022**, *22*, 9260–9267.

44. Li, G.X. *Advanced Soil Mechanics*, 2nd ed.; Tsinghua University Press: Beijing, China, 2016; pp. 62–64.